Size dependent structural, energetic and spectroscopic properties of the MoS_3 polymorphs

Amit Sahu[1,2] , Stephan N. Steinmann[2] and Pascal Raybaud[1,2]*

[1]IFP Energies Nouvelles, Rond-point de l'échangeur de Solaize, BP3 - Solaize 69360 (France)

[2]Univ Lyon, ENS de Lyon, CNRS UMR 5182, Laboratoire de Chimie, 69342 (France)

ABSTRACT: In spite of the attractive interest of a-MoS_3 based nanomaterials, the amorphous nature of the MoS_3 phase makes it challenging to control and understand its chemical reactivity. In particular, the type of the structural building unit such as Mo_3 triangular vs. Mo chain is still debated, while the ambivalent interpretation of the nature of sulfur species (S^{2-}, S_2^{2-}) and Mo-Mo bonds leads to ambiguous interpretations of spectroscopic data and reactivity. By density functional theory (DFT), we simulate the energetic, structural, and spectroscopic features of relevant 0D-, 1D- and 2D-MoS_3 triangular, chain-like polymorphs, including unprecedented ones (ring, wave and helix) and revisit the interpretation of EXAFS, IR-RAMAN, and XPS experimental data. We analyze how Mo_kS_{3k} clusters of a few *k* atoms may grow up to infinite MoS_3 polymorphs (periodic replica). The evolution of the growth energy and the computed IR spectra within density functional perturbation theory level suggest the coexistence of various polymorphs in the MoS_3 phase as a function of sizes. Molecular dynamics simulations reveal how the small triangular Mo_kS_{3k} oligomers may transform into a more condensed MoS_3 patches resembling embryos of the 2D 1T'-MoS_2 phase. Finally, we discuss some plausible transformation pathways from one polymorph to another.

KEYWORDS: MoS_3 polytypes, MoS_2, density functional theory, Infra-Red, Thermochemistry, Growth

INTRODUCTION

Over the past few decades, amorphous MoS_3 (*a*-MoS_3) based nanomaterials have gained great attention from the scientific community because of their versatile properties valuable for industrial applications as well as for numerous emerging applications in new energies. The *a*-MoS_3 phase was shown to play a key role as electro-and photochemical (pre-)catalysts for hydrogen evolution reaction (HER).[1–3] It was also found to exhibit attractive capacity and rate capability when used in electrodes materials for batteries.[4–8] The use of *a*-MoS_3 was also suggested to improve the recovery of Hg capture from flue gas.[9,10] Finally, in the synthesis of industrial MoS_2 based catalysts used in hydrodesulfurization (HDS), *a*-MoS_3 is known to be a key precursor formed during the activation of the 2H-MoS_2 nano-crystalline phase.[11,12]

Many of these interesting properties of *a*-MoS_3 are supposed to originate from its intriguing amorphous 1D- or 2D-nano-structure where Mo atoms are interconnected by various types of sulfur atoms such as S^{2-} and S_2^{2-} species. These versatile species are suspected to improve the reactivity towards the different key reactants involved in the targeted applications: diffusion of cations in battery materials[6,7], activation of H_2 in HER[13–16] and HDS reaction[17], and specific interaction with Hg.[9]

Nevertheless, in spite of these wide range of potential applications of MoS_3, challenging questions remain open regarding its structural, electronic, and spectroscopic features. Indeed, the amorphous nature of MoS_3 makes it difficult to precisely identify the type and local structure of these active sulfur sites in order to better rationalize their reactivity.

Since the early 70' several experimental studies were devoted to the a-MoS_3 phase.[18–33] However, the atomistic picture of a-MoS_3 remains uncertain. In particular, there is historical and still vivid debate on the nature of the structural building block, either Mo_3 triangular[27,34,35] or Mo chain-like,[19,23,28,29] and the oxidation states of Mo atoms which also depends on the characterization techniques used.

Earlier studies based on radial distribution function (RDF), extended X-ray absorption spectroscopy (EXAFS), magnetic susceptibility and X-ray photoelectron spectroscopy (XPS) proposed a chain-like model along with the Mo oxidation state five.[19,23] EXAFS data suggested that two types of Mo-Mo bonds would be present in *a*-MoS_3 : one short bond at 2.74 Å and one long at 3.14 Å.[19,21] So every metal atoms would be involved in a Mo-Mo pair generating alternatively short Mo-Mo bond, and longer Mo-Mo bond connecting each dimer. However, many subsequent EXAFS studies identified only one short Mo-Mo bond at 2.75-2.77 Å.[28,31,33,36] Based on an extensive EXAFS study, Cramer et al. proposed two possible models a chain-like and cyclic Mo_3 model with two possible oxidation states $Mo^{5+}(S^{2-})_2(S_2^{2-})_{1/2}$ and $Mo^{4+}(S^{2-})(S_2^{2-})$ respectively, admitting that they cannot be distinguished by EXAFS.[36] By combining low angle X-ray diffraction (XRD) and theoretical models, Chien et al. preferentially suggested a Mo^{5+} chain like model with two Mo-Mo bonds: one short at 2.80 Å and a very long one at 3.40 Å.[23]

A combined neutron diffraction study and reverse Monte Carlo simulation method study by Hibble et al.[37] contradicted the previous studies by proposing a chain like model of $Mo^{4+}(S^{2-})(S_2^{2-})$ with only one short Mo-Mo distance. This result was consistent with earlier XPS emission and absorption studies analyzing the nature of the covalent nature of chemical bonding in MoS_3 and concluding that Mo with formal oxidation state of +4 was more plausible.[38]

IR and Raman investigations on a-MoS_3 and poorly crystalline MoS_2 provided other interesting insights into the features of MoS_3 phase.[20] The characteristic peak at 522 cm^{-1} was assigned to S-S stretching present in MoS_3. Based on XPS and IR analyses, Weber et al. proposed a triangular model inspired by Mo_3 clusters also argued that Mo has +4 formal oxidation state and identified the presence of various S species such as S^{2-} and S_2^{2-} ligands. By IR analysis, the main observed bands at 545, 520 and 470 cm^{-1} were assigned to $(S\text{-}S)_{br}$, $(S\text{-}S)_t$ and $(Mo\text{-}S)_{ap}$ on the basis of a $(NH_4^+)_2[Mo_3S_{13}^{2-}]$ reference compound. This interpretation must be taken with care due to charge and over-stoichiometry of $[Mo_3S_{13}]^{2-}$, as we will discuss below.[27]

Within the context of HER, Tran et al.[3] provided recently for the first time high resolution HAADF-STEM images of the MoS_3 structures highly dispersed on carbon materials. This analysis suggested that there would be an oligomeric arrangement of triangular Mo_3 cluster units in a one-dimensional quasi-linear or branched chain.[3]

Most experimental investigations which attempted to rationalize their observation refer either to the linear or triangular building blocks without clear justification. At the same time, there exists very few theoretical studies devoted to the structural resolution and most of the existing ones also assumed one type of structure. Considering quantum simulation dedicated on the MoS_3 structure, Jiao et al.[35] simulated four possible triangular Mo_3S_9 structures as empirically proposed earlier by Weber et al.[27] It was found in particular that the most stable structures significantly reconstruct from the initial structure proposed by Weber et al., while the corresponding formal oxidation state of Mo shifts from +4 to +4.67. In the lowest energy structures, short and long Mo-Mo distances are close to EXAFS data. However, due to the strong distortion of the clusters, it is difficult to compare the calculated vibrational frequencies with the experimental IR spectrum.[35] Other quantum simulations investigating the reactivity of the MoS_3 phase assumed a Mo_3 triangular model, without clear justification of it.[39,40]

As a consequence, there is a clear lack of accurate atomic scale's insights into the structural and spectroscopic properties of the a-MoS_3 phase. Density functional theory (DFT) provides a powerful formalism to revisit the empirical proposals formulated since the 70's.

In this work, by means of DFT calculations, we will investigate the previously proposed chain-like or triangular structures of MoS_3. Moreover, we will also shed light on some unprecedented 0D-2D-nano-structures of the MoS_3 polymorphs. To validate the reliability of the newly proposed structures, we will analyze first the various structures and compare them with available EXAFS data. Then, the relative stability of the various polymorphs will be determined as a function of sizes. Thirdly, we will simulate IR spectra of these models by density functional perturbation theory (DFPT) approach and compare them with a reference experimental IR spectrum of bulk-MoS_3.[27] After a brief discussion of the corresponding XPS signals, we finally propose the possible transformation of MoS_3 polymorphs upon oligomerization.

COMPUTATIONAL METHODS

For all the calculation, density functional theory (DFT) as implemented in VASP[41–43] has been used relying on the Perdew-Burke-Ernzerhof (PBE)[44] functional within the framework of generalized gradient approximation (GGA). The long-range interactions were included through a density-dependent dispersion correction (dDsC)[45,46]. The projector augmented-wave (PAW) method[47] was chosen to describe the electron-ion interaction. The kinetic energy cut-off for the plane-wave basis set has been fixed at 500 eV. Furthermore, for the minimization of the electronic energy, a Gaussian smearing with a width of 0.2 eV was chosen, while a mixture of the blocked-Davidson scheme and residual minimization method direct inversion in the iterative subspace has been applied. Spin-polarized calculations were performed to obtain the ground state of the clusters. Brillouin zone integration has been adapted as a function of each simulated system either cluster or periodic structure.

To represent the MoS_3 polymorphs, we simulated two types of molecular models: Mo_kS_{3k} clusters of various finite sizes and periodic structures of infinite size in one dimension. A large vaccume has been used, to minimize the spurious interections with neighboring images, along the nonperiodic directions of the respective models. To optimize the structures of the various polymorphs, the conjugate gradient algorithm was used. Electronic and geometric convergence cut-off has been set to 10^{-6} eV and 0.02 eV/Å, respectively. For the clusters' geometry optimization, a large cubic supercell was used to avoid the spurious interactions of the clusters with its periodic images. For the periodic structures, the ionic positions and cell parameter along the periodic replica have been optimized.

The exploration of some complex structures has been refined by ab initio molecular dynamics (AIMD) with the scaled velocity Verlet algorithm to solve Newton's equations of motions (time step of 5 fs and T = 1000 K).

For frequency calculations, the structures have been optimized with tighter convergence criteria such as 10^{-7} eV for electronic properties and 0.01 eV/Å for geometry. To calculate the frequencies and corresponding infra-red intensities, the linear response method with density func-

tional perturbation theory (DFPT) has been used as implemented in VASP.[48] We convoluted the IR intensity peaks by normal distribution with the variance 80 cm^{-1} to compare with the experimental IR.

To calculate the core-level binding energy (ΔBE), we use Janak-Slater transition state approach[49–51], where half electron is shifted to the lowest unoccupied molecular orbital (LUMO) from its core rather than creating a full core-hole. We compare this ΔBE with available XPS data.

For determining the thermodynamic stability of the various oligomers, the following equation has been used to calculate the relative growth energy ΔE at 0 K:

$$Mo_3S_9 \rightarrow \frac{3}{k} Mo_kS_{3k} \quad (1)$$

$$\Delta E = \frac{3}{k}\left[E(Mo_kS_{3k}) - E(Mo_3S_9)\right] \quad (2)$$

where $E(Mo_kS_{3k})$ is the electronic energy of the Mo_kS_{3k} cluster or periodic structure, and $E(Mo_3S_9)$ is the energy of Mo_3S_9 cluster used as a reference. The effect of zero-point energy, thermal corrections, and entropy, have be included to calculate the free energy variation (details are given in Supporting information SI.3) :

$$\Delta G = \frac{3}{k}\left[G_{vib}(Mo_kS_{3k}) - G_{vib}(Mo_3S_9)\right] \quad (3)$$

We have assumed that the Mo_kS_{3k} clusters or infinite structures are immobile, and thus they have no translational and rotational contributions.

RESULTS

Structure Analysis

oD- and 1D-model of triangular oligomers (TO). Inspired by the earlier experimental work by Weber et al.[27], we first optimized the numerous possible structures of the Mo_3S_9 triangular monomers. All these structures differ by the nature, number and location of sulfur species:

- S_2^{2-} dimers, either on top (also called μ_1-S_2 in what follows) or in bridging site (μ_2-S_2),
- S^{2-} atoms, either on top (μ_1-S), or in the bridging site (μ_2-S) or in the hollow site (μ_3-S).

The most stable structure is shown in Figure 1 a), while other metastable structures with relative energies are given in Figure S1. This stable structure exhibits :

- two S_2^{2-} dimers : one μ_1-S_2 and one μ_2-S_2,
- four S^{2-} atoms : two μ_1-S, two μ_2-S and one μ_3-S.

None of the empirically proposed structures by Weber et al.[27] corresponds to the most stable one: their energy is at least +0.65 eV higher than the one reported in Figure 1 a). Weber's proposals were made on the assumption of the experimentally observed +4 oxidation state of Mo. Actually, our minimal energy structure of Mo_3S_9 exhibits an average formal oxidation state of +4.67 (assuming a formal 2 e^- charge for the S-atom and S_2 dimers). Previous DFT calculations also showed that Weber's structures are subject to strong reconstructions, and the resulting Mo exhibits formal oxidation states higher than +4.[35] This apparent discrepancy indicates that such Mo_3S_9 triangular monomers are not the dominant species in a-MoS_3. Nevertheless, they might co-exist with other oligomeric structures with an average oxidation state close to +4.

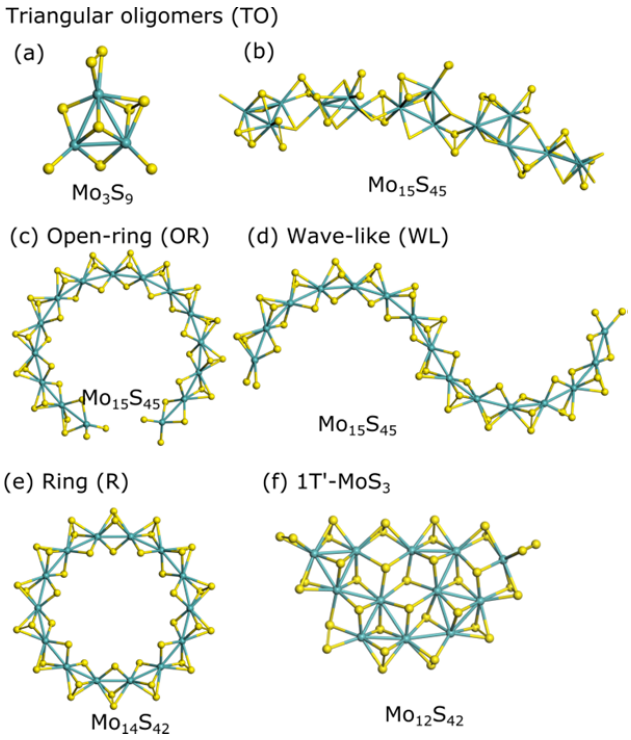


Figure 1 (a) Various oD-MoS_3 nano-structures: Triangular monomer Mo_3S_9 and triangular oligomers (TO) $Mo_{15}S_{45}$, (c) open ring (OR) conformer, (d) Wave like (WL), (e) Ring (R) and (f) 1T'-MoS_3 (see text for explanation).

Interestingly, our most stable Mo_3S_9 structure exhibits two distinct types of Mo-Mo bond length: one short Mo-Mo bond at 2.72 Å and two long Mo-Mo bonds at 2.96 Å which are compatible with some experimental EXAFS studies: 2.75 and 3.16 Å, respectively,[19,36] although we noticed a slight underestimation of 0.18 Å for the long Mo-Mo bond. Also, the mean Mo-S bond length (2.35 Å) is in close agreement with the experimental value (2.41 Å).

However, as suggested experimentally, *a*-MoS_3 could actually consist of larger oligomers made of Mo_3S_9 triangular clusters interconnected by S species. [3,27] Exploring the size effects on triangular oligomers (TO) requires the simulations of various TO conformers. For Mo_6S_{18} this revealed that the interconnection of two Mo_3S_9 triangular units occurs through one S_2 dimer and one S atom (initially μ_2-S) becoming μ_3-S (Figure S2). Hence, this interconnection does not involve only one or two S-atoms as initially suggested,[27] but three S-atoms. This structural trend is further confirmed for the larger oligomers Mo_9S_{27},

$Mo_{12}S_{36}$ and $Mo_{15}S_{45}$ (Figure S3-a and Figure 1 b). The average formal oxidation state of Mo in these oligomeric structures continuously decreases from +4.67 for Mo_3S_9 to +4.16 for $Mo_{15}S_{45}$ TO. This evolution is due to the vanishing contribution of μ_1-S_1 species located at edges when size increases. Note that in the following, we will call "edges" the two terminal units of the chain like model.

To go beyond the 0D structures, we have optimized the corresponding 1D structure of TO systems. According to the spatial rotation of each Mo_3S_9 triangular unit along the TO chain, the smallest periodic structure allowing the chain interconnection between two neighboring supercells was found for $Mo_{18}S_{54}$ (Table S2 and Figure 2 a). For this 1D TO-periodic (TO-P) chain, no μ_1-S species remains as a consequence of periodicity. Moreover, the mean Mo oxidation state reaches the limit of +4 for TO-P, while it is 4.11 for $Mo_{18}S_{54}$, both of which are very close to the experimental value.[27]

Considering the local interatomic distances, the short and long Mo-Mo and Mo-S bond-lengths slightly expand as a function of the oligomer size (Table S2). For the $Mo_{18}S_{54}$ TO-P structure, we determine these bond lengths (Table 1) by calculating the pair correlation functions (PCF, Figure S8). The short Mo-Mo bond length is about 2.76 Å, and the long Mo-Mo bond becomes 3.08 Å which is in closer agreement with the experimental EXAFS data (Table 1).[19] As the size of TO increases, the long Mo-Mo bond present in triangular monomers such as Mo_3S_9 shortens (Figure S4 a) while the long Mo-Mo bond is located at the interconnection of two triangular monomers along the chain. The mean Mo-S bond length also slightly expands to 2.42 Å with the size increase, in good agreement with EXAFS.

At this stage, we must recall that many EXAFS studies do not report the long Mo-Mo bond length[28] which may raise question about the precise assignment of the structure on the basis of the Mo-Mo distance. Therefore, we also investigate alternative structures below.

0D and 1D-Chain like models: open-ring (OR), wave-like (WL), linear (L) and helical (HL). Within the chain-like models, two competing ones were initially proposed: one strictly linear made of $Mo^{5+}(S^{2-})_2(S_2^{2-})_{1/2}$[19,23] and one distorted made of $Mo^{4+}(S^{2-})(S_2^{2-})$.[37] Hence, we started by investigating two periodic structures of strictly linear chain like models involving either $Mo^{5+}(S^{2-})_2(S_2^{2-})_{1/2}$ or $Mo^{4+}(S^{2-})(S_2^{2-})$. For the Mo^{5+} model, the optimized structure (Figure S7 b) confirm the presence of two Mo-Mo bond lengths (2.70 and 3.28 Å) compatible with Ref.[23] while for the Mo^{4+} model (Figure 2 b), the structure exhibit one short Mo-Mo bond only (2.90 Å) longer than the one usually reported by EXAFS (Table 1).[28] Moreover, the DFT energies show that the Mo^{4+} model is more stable by 0.11 eV per MoS_3 unit. This preliminary result may be consistent with Hibble's proposal.[37]

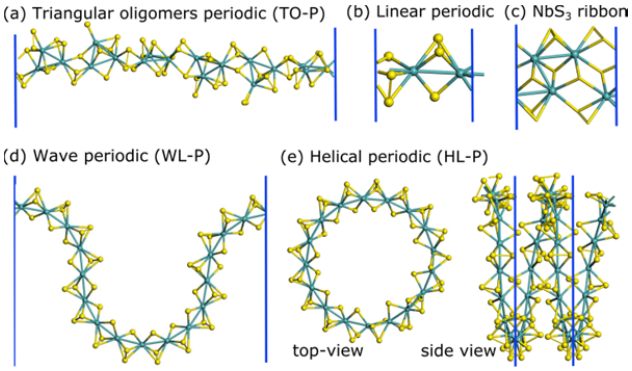


Figure 2 : Various MoS_3 nanostructures : a) Triangular oligomers $Mo_{18}S_{54}$ (TO-P), (b) Linear periodic Mo_2S_6 (L-P), (c) NbS_3-ribbon (Mo_4S_{12}) (d) $Mo_{16}S_{48}$ Wave-like (WL-P), and (e) $Mo_{17}S_{51}$ Helical (HL-P). Direction perpendicular to the blue lines is the direction of periodicity.

Releasing the periodic constraint, any attempt to stabilize a finite size Mo_kS_{3k} clusters of $Mo^{5+}(S^{2-})_2(S_2^{2-})_{1/2}$ formal unit relaxed into a curved chains of $Mo^{4+}(S^{2-})(S_2^{2-})$: open-ring (OR, Figures 1 c and S3 b) and wave-like (WL, Figures 1 d and S3 c). The observed curvatures are induced by the relative position of two successive S_2 dimers. In OR, the relative tilting angle of two successive dimers is always ~60° (Figure S5). When this alternate tilting of two successive S_2 dimers is locally broken at a chain's point, the chain curvature changes which leads to a WL-type structure (Figure 1 d). In the extreme case of a linear chain, the relative tilting angle between two successive dimers is ~90° (Figure S5).

As for TO polymorphs and linear chain, we explore the construction of 1D-periodic structures for the curved structures. One original structure directly inherited from OR, is the closed ring (R) represented for $Mo_{14}S_{42}$ in Figure 1 e, which resembles MoS_2 nanotubes.[52] In that case, OR is locked by bridging the two edges through Mo-S-Mo bonds involving the dangling S and S_2 species at OR edges. Nevertheless, this lock of the cycle only occurs for an even number of Mo atoms because of the tilting alternation of the S_2 dimer invoked before. The cycle tension depends on the size and, hence, the relative stability of R models depends on their sizes (Figure S3 e). OR and R structures exhibit one type of short Mo-Mo bond length (about 2.72-2.79 Å) with very small variation according to size (Table S2).

Table 1 : Mo-Mo and Mo-S bond lengths (in Å) for various types of MoS_3 polymorphs.

Bond	TO-P	Ring	WL-P	HL-P	L-P	1T'-like	EXAFS*	EXAFS**
Mo-Mo_{short}	**2.76**	**2.75**	**2.77**	**2.76**	**2.90**	**2.79**	**2.75**	**2.75**
Mo-Mo_{long}	**3.08**	--	--	--	--	**3.16**	**3.16**	--
Mo-S_{short}	**2.27**	**2.29**	**2.30**	**2.31**	**2.31**	**2.33**	--	--
Mo-S_{long}	**2.46**	**2.46**	**2.45**	**2.46**	**2.46**	**2.47**	--	--
Mo-S_{avg}	**2.42**	**2.39**	**2.39**	**2.40**	**2.40**	**2.44**	**2.44**	**2.44**

*according to Ref.[36] , ** according to Ref.[28]

1D periodic structures (WL-P) containing various numbers of Mo per unit cell depending on the wave amplitude were optimized (Figure S6 and Figure 2 d). Finally, a more complex structure consists of a helical periodic (HL-P) structure as shown in Figure 2 e, which results from 3D distortion of the R structures induced by the change of the relative orientation of successive S_2 dimers. Interestingly, these more complex 3D structures are very similar to the one proposed by Hibble et al.[37] Table 1 shows that these periodic structures also exhibit one short Mo-Mo bond (about 2.76-2.77 Å) as for OR and R structure. The Mo-Mo PCF analysis (Figure S8) reveals that the structural feature of this polymorph family clearly differs from TO. The mean Mo-S bond length is ~2.40 Å, while the S-S bond length in S_2 bridging dimer is ~2.05 Å (whatever the size, except for the smallest constrained Mo_6S_{18} ring, Table S2).

Comparing the Mo-Mo and Mo-S bond-lengths of various explored structures with EXAFS data (Table 1), we observe that all the chain like structures (linear, WL, WL-P, HL-P and R) have only one Mo-Mo bond in contrast with TO. This type of polymorph would thus explain the fact that EXAFS data do not identify the longer Mo-Mo distance in some experimental MoS_3 samples, whereas it may exist in other ones which would be of TO type.[28]

MoS_3 patches with 1T'-MoS_2 like structure. Ab-initio molecular dynamics (AIMD) was performed to explore if new possible structures can be revealed. Starting AIMD from TO metastable conformers identified at 0 K after geometry optimization (such as the one highlighted for Mo_6S_{18} in Figure S2), the system explored rapidly a large configurational space. The structural evolutions of the Mo_6S_{18} and Mo_9S_{27} oligomers (Figures S9 and S10) show that the triangles rapidly interconnect by one μ_2-S_2 species plus one μ_3-S species as we found by static optimization. Moreover, the dynamic evolution proceeds further and reaches, after a few picoseconds, more condensed rearrangements exhibiting respectively 4 and 8 adjacent triangular clusters interconnected by μ_3-S species. Figure S3 illustrates the final products obtained after quenching at 0 K both Mo_6S_{18} and Mo_9S_{27} condensed structures. For $Mo_{12}S_{36,}$ the corresponding optimized structure is represented in Figure 1 f. The structural patterns of these triangular Mo_3 in Mo_6S_{18}, Mo_9S_{27} and $Mo_{12}S_{36}$ are very similar to the one found in the 1T' polymorph of MoS_2, where μ_3-S atom are located in hollow sites of Mo_3 triangles, with an alternate position either above or below the Mo plane. Note, however, that the edge/surface ratio needs to be appropriate to keep the nominal MoS_3 stoichiometry. Indeed, as discussed below, a nanoribbon with similar stability satisfies this constraint. Actually, the PCF analysis of $Mo_{12}S_{36}$ reveals that two main Mo-Mo distances are observed: one short at 2.79 Å and one long at 3.16 Å (Table 1 and Figure S4). This implies that the $Mo_{12}S_{36}$ condensed structure is actually closer to the 1T' phase of MoS_2 with specific ordering of the contracted and expanded Mo_3 triangles within the structure, whereas one single long Mo-Mo bond is reported for the 1T phase.[53] Interestingly, the NbS_3 structure could also exhibit a nano-ribbon made of two infinite Nb rows arranged in similar way as in Mo_6S_{18} cluster.[54,55] The simulation of an analogous 2D-periodic MoS_3 nano-ribbon (Figure S11) reveals the presence of short Mo-Mo distances co-existing with significantly longer one.

This structural analysis indicates that if EXAFS reports the presence of two types of Mo-Mo bonds (short or long), it is difficult to discriminate whether they are due to the formation of one single polymorph or a mixture of polymorphs. To go beyond, we evaluate in what follows the relative stability of these various polymorphs.

Energetics analysis. Figure 3 reports the growth energy (at 0 K, without ZPE corrections) as a function of the size of the various polymorphs described in the previous section. The impact of ZPE and temperature is reported in Figure S12 which shows that it is more pronounced for the larger size clusters as compared to smaller size ones. In most of the cases, entropy and thermal corrections stabilize the clusters for higher temperature. However, these thermal and entropic effects influence only moderately the main energetic trends, so we present the results considering 0 K energies in what follows.

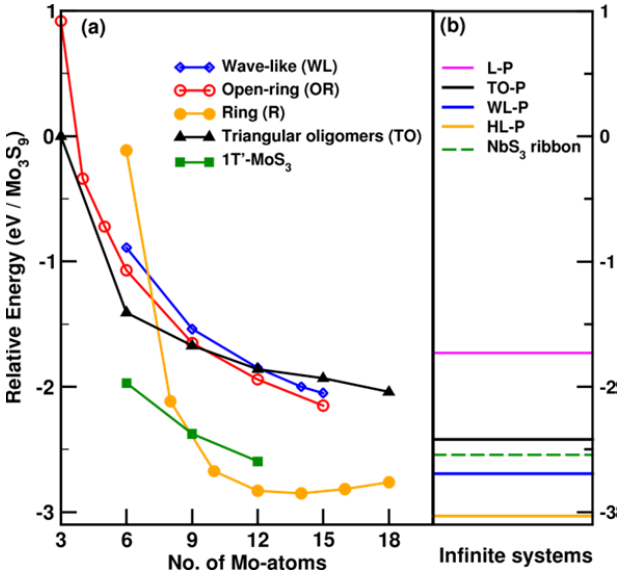


Figure 3 : Growth energies of (a) 5 relevant types of MoS_3 polymorphs as a function of size (reference energy is the Mo_3S_9 triangular cluster), (b) corresponding periodic structures: L-P, TO-P, WL-P, HL-P and NbS_3-like MoS_3 ribbon.

On the growth energy diagram (Figure 3), as expected all curves (except the one of R) exhibit a continuously decreasing trend as a function of size, with a continuously decreasing slope. However, even for large sizes considered in the present study (up to 16 Mo), a plateau in energy is not yet reached and the asymptotic limit value for infinite size can only be estimated of the polymorphs placed in periodic supercells as described before for L-P, TO-P, WL-P and HL-P.

The OR and WL polymorphs share a similar internal structure. Hence, they are nearly iso-energetic and their relative energy remains constant as a function of the size. Nevertheless, WL is slightly less favored compared to OR due to the point defects induced by the change in the tilting angle of the S_2 dimer (as described before).

The relative energies between other families of MoS_3 polymorphs of different types are, however, size dependent. Considering first the 0D TO and OR structures, the energy values of the smallest Mo_3S_9 and Mo_6S_{12} clusters reveal that TO is strongly stabilized with respect to OR by ~1 eV for Mo_3S_9. By contrast, the infinite TO-P polymorph is less stable than WL-P and HL-P. The inversion of stability between TO and OR or WL occurs for 9-12 Mo atoms. For larger oligomers, OR or WL are more stable.

If we consider the lowest energy L-P model (pink in Figure 3), it is obvious that it is significantly less stable than all other polymorphs and cannot be considered relevant for the a-MoS_3 phase. Our more stable models preferentially exhibit curved or bent chains such as found in OR/WL/HL. This is in qualitative agreement with Hibble's bent chain models exhibiting numerous elbows.[37]

The most striking energetic result concerns the R model. Indeed, for size greater than 8 Mo the R models emerge as the thermodynamically most stable arrangement except for the HL-P polymorph which is competitive with the lowest energy R structure reached at 14 Mo. The R models are strongly stabilized with respect to OR due to the absence of edge energies after ring closure. This edge effect is generally stronger for OR/WL than for TO which explains also the higher energies of OR/WL for small sizes. In agreement with these considerations, the stabilization of the periodic TO-P system with respect to the larger TO is less pronounced than for WL. The periodicity in WL-P also enables to wipe this edge effect out. So the stability of WL-P may compete with R, when the ring-strain is non-negligible.

As we have explained in the previous section, OR may grow in a helical structure HL/HL-P, which has the lowest energy we could identify for MoS_3 models. This stabilization is induced by the close proximity of two helical rings which supplements Van-der-Waals interactions, not present in any other periodic system.

Finally, Figure 3 demonstrates that the stability of the 1T'-like MoS_3 polymorph, including the NbS_3-like nano-ribbon, strongly competes with many other phases. This result is also consistent with the AIMD simulation which highlighted the fast transformation from TO into 1T'-like MoS_3 clusters. For sizes up to 12 Mo atoms, 1T'-like MoS_3 clusters are more stable than OR/WL and TO. For the 1D structures, the MoS_3 nano-ribbon is slightly more stable than TO-P but less stable than WL-P. Hence, here again this would mean that size effect will modulate the relative stability of this polymorph which would be favored at small sizes.

Spectroscopic analysis

IR spectrum of TO and 1T'-MoS_3 polymorphs: As a preliminary important analysis detailed in Supplementary Information SI.4, the empirical IR assignment of MoS_3 based on $(NH_4^+)_2[Mo_3S_{13}]^{2-}$ reference compound[27] must be questioned due to the effects of the $2e^-$ charge and S/Mo over-stoichiometry involved in this reference compound. Weber et al.[27] have assigned the two characteristic peaks at 520-525 cm^{-1} to μ_1-S_2 and 545-555 cm^{-1} to μ_2-S_2. While the simulation confirms that in $[Mo_3S_{13}]^{2-}$ the two characteristic peaks at 520-525 cm^{-1} and 545-555 cm^{-1} can be

assigned to μ_1-S_2 and to μ_2-S_2 respectively, the S-S vibrational frequencies of these two species cannot be easily distinguished anymore in the neutral $[Mo_3S_9]^0$ due to the significant shift of the S-S frequency in μ_1-S_2 with or without charge. Moreover, μ_1-S or μ_2-S species exist in $[Mo_3S_9]^0$ as well as in the larger TO previously identified, while they are not present in $[Mo_3S_{13}]^{2-}$.

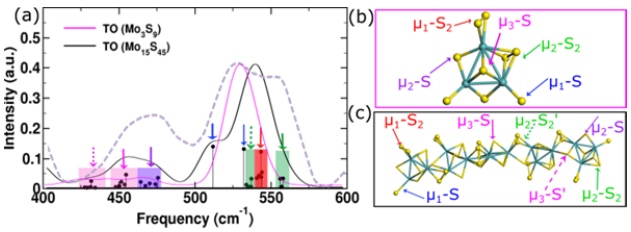


Figure 4 : (a) IR spectra of Mo_3S_9 (pink line), TO $Mo_{15}S_{45}$ (black line) and 1T'-MoS_3 cluster (blue line). Coloured arrows point the contributions of the various S species as defined in the structural models of (b) triangular Mo_3S_9 and (c) TO $Mo_{15}S_{45}$. All simulated spectra have been renormalized while keeping the highest intensity peak fixed. Experimental IR spectrum (dashed line) from ref.[27]

The simulation of IR spectra performed (e.g. Figure 4 a), are compared with the *a*-MoS_3 bulk IR spectrum provided in Ref.[27], similar to other published spectra.[3,20] Since the region below 400 cm^{-1} involves mixed vibrational modes of Mo-S and Mo-Mo, we focus in the following on the region 400-600 cm^{-1}. As we expect from the preliminary analysis of Mo_3S_9, all modes involving S_2 dimers such as μ_2-S_2 or μ_1-S_2 appear between 535-558 cm^{-1} (Table S4). For TOs larger than Mo_3S_9 (including $Mo_{15}S_{45}$ in Figure 4), two types of μ_2-S_2 exist: one located on each triangular cluster (545-558 cm^{-1}) and the one at the interconnection of two triangles (535-539 cm^{-1}). Furthermore, μ_1-S_2 appears in between two types of μ_2-S_2 (538-546 cm^{-1}) and exhibits the highest intensity of the S_2 species. Since the frequencies of μ_2-S_2 and μ_1-S_2 are very close, they produce a single broad peak in this spectrum region. Thus, considering only these two S species, it is impossible to explain the origin of the two high intensity peaks revealed in the 500-575 cm^{-1} region of the experimental IR spectrum. However, the two μ_1-S_1 species of the triangular Mo_3S_9, give rise to two high intensity peaks at 512 cm^{-1} and 532 cm^{-1} which may thus contribute to the region observed in the experimental data at about 525 cm^{-1}. This interpretation has never been proposed in the experimental literature due to the use of the $(NH_4^+)_2[Mo_3S_{13}^{2-}]$ reference, which does not contain μ_1-S_1 species. Figure S13 illustrated the effect of TO size on the evolution of the IR spectra: the intensity of the first μ_1-S_1 high intensity peak decreases with increasing size because μ_1-S_1 are located at TO edges.

Finally, in the broad region between 425 and 475 cm^{-1}, the simulation reveals a contribution of three types of species:

- μ_3-S on each triangular cluster at ~430 cm^{-1},
- μ_3-S at the interconnection of the triangular clusters at ~425 cm^{-1},
- μ_2-S species on each triangular cluster at 446-475 cm^{-1}.

Increasing the size of TO up to the infinite TO-P enhances the intensity of this broad low wave number region with respect to the 500-575 cm^{-1} region (Figure S13).

However, considering one single type of TO polymorph makes it difficult to recover the experimental IR spectrum. As the previous energetic analysis showed that TO polymorphs are less stable for large size than chain like ones (OR, R, WL) or 1T'-MoS_3 clusters, we investigate their spectroscopic features next.

IR spectrum of chain like (OR, R and WL) polymorphs. The simulated spectra of chain like models OR and R reveal that they exhibit all very similar features (Figures S14 and S15): as an example, R $Mo_{14}S_{42}$ is also reported in Figure 5. It is important to recall that no μ_1-S_2 species are present and that μ_2-S_2 and μ_2-S are predominantly located in the internal chain (Figure 1). Thus, the simulated spectra are dominated by one intense region between 531 to 547 cm^{-1} due to μ_2-S_2 species (Table S5). Increasing the size of OR and R induces a slight shift to higher frequencies of the μ_2-S_2 region. This trend is correlated to the slight increase of the S-S bond length (from 2.053 Å to 2.067 Å) when the size increases. OR also contains 4 μ_1-S at edges with a peak at ~508 cm^{-1}, which intensity decreases with increasing size due to the loss of edge effects. Finally, the μ_2-S modes contribute to the broad region 450-475 cm^{-1}, depending on sizes (Table S5). Due to the absence of the μ_3-S contributions and the IR intensity quenching interaction between μ_2-S species, this low frequency region is much less intense for the chain-like models than in TO polymorphs.

WL exhibits a similar trend as TO for the regions due to μ_2-S_2 and μ_2-S contributions (Figure S16). In addition, the 4 μ_1-S at edges imply the appearance of a marked shoulder around 515 cm^{-1} for the small sizes. As for OR, this edge effect vanishes for very large and infinite size, such as in WL-P. Here again, the broad region 450-475 cm^{-1} exhibits a very weak intensity. To enhance this region, one should break the high symmetry of the R, WL and OR systems by generating a helical system as shown for HL-P in Figure 5. In this case, the 3D-distortion of the chain enhances the contributions μ_2-S which are not located all perfectly located in the plane of the circular region of HL.

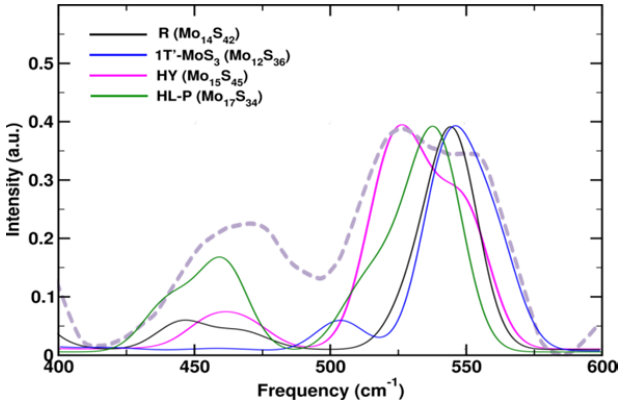


Figure 5 : IR spectrum of R, HL-P, HY, and 1T'-MoS_3 polymorphs (solid lines). All simulated spectra have been renormalized while keeping the highest intensity peak fixed. Dashed curve : experimental IR spectrum from ref.[27]

Finally, Figure 5 reports the simulated IR spectrum for the 1T'-MoS_3 cluster ($Mo_{12}S_{36}$) revealing that the predominant μ_2-S_2 species and the 2 μ_1-S_2 present at edges exhibit a slightly broad region at about 550 cm^{-1}, which matches well the high frequency region of the experimental spectrum.

DISCUSSION

Our revisited assignment of the IR spectrum of MoS_3 reveals that the higher region at 545-555 cm^{-1} is assigned to both μ_1-S_2 and μ_2-S_2 when they exist as in TO polymorphs (with at least 6 Mo), or to μ_2-S_2 only as in chain like models (R, OR, WL, HL), or to edges of 1T'-MoS_3. The IR region at 520-525 cm^{-1} is reproduced only if μ_1-S species are present either at edges of the chain like and TO models or on the triangular Mo_3S_9.

Moreover, the energetic analysis showed that TO models are thermodynamically stable only for the smallest size as Mo_3S_9, whereas for larger sizes, the chain like (OR, R, WL, HL) or the 1T'-MoS_3 cluster become more stable. Hence, the MoS_3 phase is actually constituted of various polymorphs as a function of the size of the oligomers. This is reflected in the IR spectrum resulting from the contribution of these various polymorphs. At this stage, we can propose the two following possible combinations of polymorphs:

- Triangular Mo_3S_9 (contributing to the region 520-525 cm^{-1}) and 1T'-MoS_3 cluster such as $Mo_{12}S_{36}$ or even NbS_3-ribbon for larger size (contributing to the region 545-555 cm^{-1})
- Triangular Mo_3S_9 (contributing to the region 520-525 cm^{-1}) and larger chain like models such as OR, R, WL or HL (contributing to the region 545-555 cm^{-1} and to the region 520-525 cm^{-1} when μ_1-S species are present at edges).

To further investigate the combination of Triangular Mo_3S_9 with chain like models, we simulated a Hybrid (HY) structure combining both one OR structure with two triangular Mo_3S_9 clusters located at its edges (Figure S3 d). As expected, this mixed structure recovers the two high frequency regions (Figure 5) of the experimental spectrum. The μ_1-S species of the triangular Mo_3S_9 give rise to a broad region at 520 cm^{-1} (Figure S17). In addition, one μ_1-S_2 of the triangular Mo_3S_9 and μ_2-S_2 of the triangles and of the OR chain gives rise to the upper part of the experimental spectrum (533-552 cm^{-1}). With increasing size this upper region gains relative intensity due to more numerous μ_2-S_2 contributions with respect to μ_1-S. Similarly, the lowest broad region between 450 and 500 cm^{-1} is also increasingly visible due to the increased number of μ_2-S within the chain (Figure S14). To enhance the intensity of this region 450-500 cm^{-1}, 3D-chain distortion as in HL is required.

XPS experiments of MoS_3 usually reveal two species μ_2-S_2 and μ_1-S_2 in the S 2p region with respective binding energies of 162.9 and 161.6. In other words, the corresponding relative binding energy, $\Delta BE=BE(\mu_2\text{-}S_2)-BE(\mu_1\text{-}S_2)$, is +1.3 eV.[27] The DFT calculation of the core level shift between μ_2-S_2 and μ_1-S_2 species yield a ΔBE of 1.55 eV in 1T'-MoS_3 and 1.57 eV in TO $Mo_{18}S_{54}$ (Table S3). Given the DFT accuracy, this value is in reasonable agreement with experiment.

However, in chain like models, μ_2-S_1 are present instead of μ_1-S_2 which may raise question about the coherence with XPS. Our DFT calculations show that $\Delta BE=BE(\mu_2\text{-}S_2)-BE(\mu_2\text{-}S)$ fluctuates between 1.14 and 1.65 eV for various WL and OR models. So, these models remain also compatible with the S 2p XPS spectrum, i.e., XPS does not allow to discriminate between these different models.

Regarding the μ_1-S species present at edges of TO, WL and OR, the question of the compatibility with XPS must be also addressed. Here, $\Delta BE=BE(\mu_2\text{-}S_2)-BE(\mu_1\text{-}S)$ is shifted to significantly higher energy: +2.84 eV in TO $Mo_{15}S_{45}$, +2.31 eV in WL (Mo=14) and +2.23 eV in OR (Mo = 15) also meaning that the binding energy of μ_1-S_2 is significantly greater than the one of μ_1-S. However, these μ_1-S species are not identified in the S 2p XPS spectrum. As a consequence, if these μ_1-S exist, they must be present in very low concentration, i.e., significantly smaller than the other S species. This low concentration of μ_1-S does not contradict the IR spectrum since we noticed that in our proposed models, their number is comprised between 2 and 4 per polymorph. For the model $Mo_{15}S_{45}$, this represents less than 10% of S species. Since the bulk MoS_3 phase is constituted by a distribution of polymorphs of various sizes going beyond $Mo_{15}S_{45}$, this percentage is certainly much lower. Due to the higher sensitivity of IR to these μ_1-S species, their low concentration does not prevent them to be visible in IR spectra, while they are not seen by XPS.

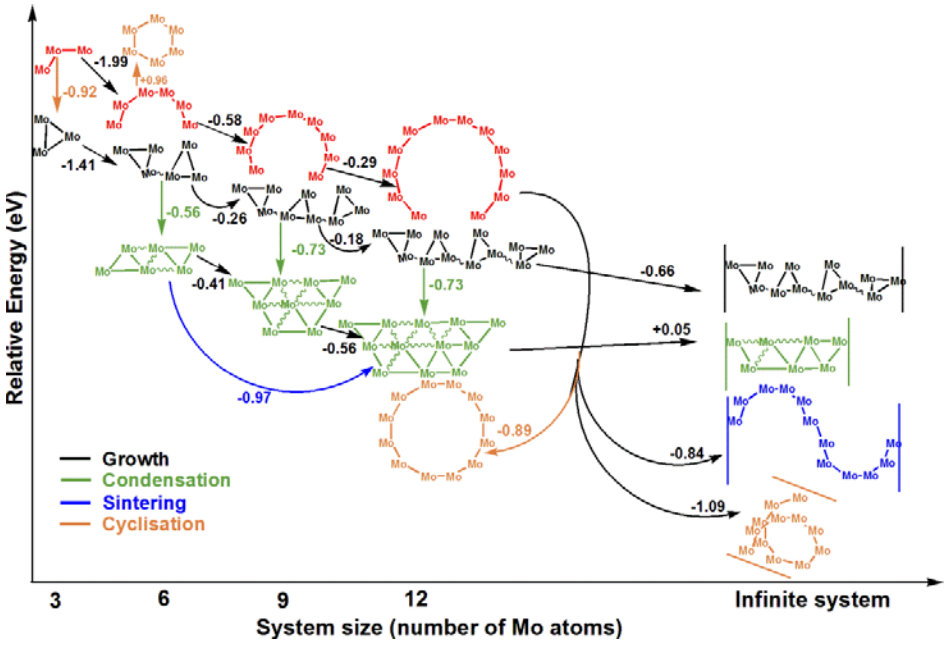


Figure 6: Possible transformation pathways of the MoS_3 polymorphs and correspondingly free energy change.

In both aforementioned combinations of MoS_3 polymorphs, the Mo-Mo bond length should exhibit the short (~2.72-2.75 Å) and long (2.96-3.16 Å) contribution as reported by some EXAFS analysis.[36] Depending on the proportion of triangular Mo_3S_9, we may suspect that the long Mo-Mo bond vanishes and the short one only becomes predominant. This could explain that other EXAFS analysis reported this short Mo-Mo bond only.[2,28,33,36] These different observations may also originate from the genesis (synthesis pathway) of the MoS_3 phase which may result in atomically different a-MoS_3 phases depending on the experimental conditions.

As illustrated by the thermodynamic energy plot (Figure 3), the triangular Mo_3S_9 is the most stable one for the smallest size. If the nucleation of MoS_3 starts from such triangular clusters, it is highly improbable that it transforms into chain like OR Mo_3S_9 because of the high reaction endergonicity (ΔG~1 eV at T=298.15 K, Figure S12). Concomitantly, if the nucleation generates OR Mo_3S_9, the reverse reaction to TO is exergonic. For larger TO, the transformation into chain like oligomers (OR, R, WL, HL) would be thermodynamically favored (Figure S12). Although further investigations are needed, it is strongly suspected that kinetic limitations of breaking several Mo-S and Mo-Mo bonds to open the interconnected triangular Mo_3S_9 clusters will prevent the transformation from TO into the chain like polymorphs. Hence, the formation of chain like polymorphs would need to be promoted during the genesis of the Mo_3S_9 embryos through specific reaction conditions (precursors or even support effects).

Assuming that the triangular Mo_3S_9 clusters are first formed, they could grow by connecting one to each other to form TO oligomers of increasing sizes. Nevertheless, as we have shown by AIMD, the small TO intermediates Mo_6S_{18}, Mo_9S_{27} and $Mo_{12}S_{36}$ are prone to be further transformed into 1T'-MoS_3 clusters through a condensation step (Figure 6). This striking dynamic behavior reveals that metastable TO conformers might readily transform into a 1T'-like MoS_3 polymorph.

The TO into 1T'-MoS_3 transformation is exergonic (ΔG~-0.56 to -0.73 eV for the three Mo_6S_{18}, Mo_9S_{27} and $Mo_{12}S_{36}$ clusters). As revealed by the AIMD simulation, this condensation mechanism occurs if the relative positions of the various dimeric and monomeric S species are optimal (supplementary information SI.2). Otherwise, it is blocked and the oligomerization of the triangular species can continue. Once the first embryos of the 1T'-MoS_3 phase are generated in the form of the structures identified by our AIMD, they could probably follow a sintering process to produce larger MoS_3 ribbons inspired by the NbS_3 structure.[25,55] Note that the transformation of TO-P into MoS_3 ribbons (NbS_3-like) is also exergonic.

In the present AIMD simulations (constant chemical composition), the obtained 1T'-like phase is thus overstoichiometric with respect to 1T'-MoS_2 and the excess S atoms are located at the edges of the 1T'-nanostructure.

Similarly over-stoichiometric triangular or hexagonal nanostructures have been reported for 2H-MoS_2.[56,57] The removal of the excess sulfur from the edge sites in the presence of H_2 as it is usual in sulfo-reductive conditions may lead to 1T'-MoS_2[12] which can further transform into 2H-MoS_2.[58–65] The easy formation of the 1T'-MoS_3 cluster also justifies the above proposal of coexistence of triangular Mo_3S_9 and 1T'-MoS_3 clusters to recover the experimental IR spectrum.

However, we cannot exclude that right from the early stage the nucleation forms a chain like cluster (if stabilized by support effect or nature of precursor) which rapidly grows by adding "linearly" other Mo atoms before transforming into TO that is energetically preferred in the gas-phase for small clusters. Furthermore, if the growth of OR proceeds further, cyclisation process from OR to R would be likely considering the significant free energy gain (ΔG~-0.89 eV at T=298.15 K, for $Mo_{12}S_{36}$). The fact that such ring structures have not been yet reported so far, may indicate that the first scenario is common. However, we propose that the improvement of synthesis or characterization methods could allow to identify the R structures. Alternatively, the a reconstruction of the terminal units of the OR structures could result in the HY structures where triangular clusters and a chain are interconnected. We have shown above that the simulated IR spectrum of these HY polymorphs is also compatible with the experimental one.

CONCLUSIONS

By means of DFT calculations, the present work provided a detailed analysis of the structural, energetic and spectroscopic properties of the a-MoS_3 amorphous phase. The challenging question of the amorphous nature of this phase was addressed by identifying several structures of possible conformers such as chain-like and triangular oligomers either previously invoked in the experimental literature or newly proposed. By simulating cluster models and periodic structures, we showed how size effects impact the relative stability of these various polymorphs.

We first ruled out the strictly linear models of $Mo^{5+}(S^{2-})_2(S_2^{2-})_{1/2}$[19,23] and of $Mo^{4+}(S^{2-})(S_2^{2-})$ which are both significantly less stable than triangular models or curved chain. The curvature is induced by specific orientation of S_2 dimers as found in open-ring (OR), ring (R), wave-like (WL) or helical (HL) structures.

For small sizes, the triangular Mo_3S_9 is more stable than the chain like models. Nevertheless, the free energy rapidly becomes favorable to chain-like models when increasing size. In particular, for the largest oligomers studied here ($Mo_{15}S_{45}$), OR and R becomes more stable than TO, while the periodic structures such WL-P and HL-P confirm that chain like models are favored.

To the best of our knowledge, the stable ring structures were never observed experimentally. So, as a first perspective to favor the formation of this appealing ring structure, we suggest that experimental studies may explore alternative synthesis pathways to prevent the formation of triangular clusters and to prompt the cyclisation process.

We proposed possible transformation pathways for the MoS_3 oligomers: from their nucleation to growth accompanied eventually by condensation and cyclization steps. In particular, AIMD simulation revealed the easy transformation of the MoS_3 TOs into a so-called "1T'-MoS_3" phase with the typical structural pattern of the 1T'-MoS_2 phase. The corresponding periodic structure should be MoS_3-ribbon inherited from the NbS_3 phase.

Our large variety of explored structures allowed to revisit the interpretation of experimental EXAFS, IR and XPS spectra. The DFPT simulation of IR spectra highlighted the particular contribution of Mo-S mode of μ_1-S species in the 525 cm^{-1} region, while the S-S modes of μ_1-S_2 and μ_2-S_2 contribute to the 550 cm^{-1} region. The core level shift calculations reveal the XPS compatibility of all S species, excepting μ_1-S species present at the edges of the chain like model or in the triangular Mo_3S_9 which, therefore, should at most exist in very low concentrations. To recover the IR spectrum, we proposed relevant combinations of polymorphs. These combinations of polymorphs may also explain why EXAFS data report either one or two types of Mo-Mo bond lengths depending on the relative concentrations of each polymorph. The curved chain-like model contains only one short Mo-Mo bond, whereas the TO model contains one short and one long Mo-Mo bond length.

This in-depths theoretical study provides a rational understanding of the amorphous MoS_3 phase which could be useful for improving its reactivity as well as the genesis of MoS_2 phases (1T or 2H) used in many applications : hydrotreatment, hydrogen evolution reaction, storage materials...

ASSOCIATED CONTENT

Supporting Information. SI.1 Structural analysis, SI.2 Ab-initio molecular dynamics, SI.3 Thermochemistry, SI.4 Spectroscopic analysis. CIF files for relevant structures. This material is available free of charge via the Internet at http://pubs.acs.org.

AUTHOR INFORMATION

Corresponding Author

*pascal.raybaud@ifpen.fr

Author Contributions

The manuscript was written through contributions of all authors. All authors have given approval to the final version of the manuscript.

Funding Sources

Any funds used to support the research of the manuscript should be placed here (per journal style). Calculations were performed using HPC resources (Jean Zay and Occigen) from GENCI-CINES (Grant A0020806134) and ENER 440 from IFP Energies nouvelles. This work is part of the "RatiOnAl Design for CATalysis" (ROAD4CAT) industrial chair, project IDEXLYON funded by the French National Research Agency (ANR-16-IDEX-0005) and the Commissariat-General for

Investment (CGI) within the framework of Investissements d'Avenir program ("Investment for the future").

REFERENCES

(1) Merki, D.; Fierro, S.; Vrubel, H.; Hu, X. Amorphous molybdenum sulfide films as catalysts for electrochemical hydrogen production in water. *Chemical Science* **2011**, *2*, 1262–1267.

(2) Tang, M. L.; Grauer, D. C.; Lassalle-Kaiser, B.; Yachandra, V. K.; Amirav, L.; Long, J. R.; Yano, J.; A, P. A. Structural and Electronic Study of an Amorphous MoS_3 Hydrogen-Generation Catalyst on a Quantum-Controlled Photosensitizer. *Angew Chem Int Ed Engl* **2011**, *50*, 10203–10207.

(3) Tran, P. D.; Tran, T. V.; Orio, M.; Torelli, S.; Truong, Q. D.; Nayuki, K.; Sasaki, Y.; Chiam, S. Y.; Yi, R.; Honma, I. *et al.* Coordination polymer structure and revisited hydrogen evolution catalytic mechanism for amorphous molybdenum sulfide. *Nat. Mater.* **2016**, *15*, 640–646.

(4) Matsuyama, T.; Hayashi, A.; Ozaki, T.; Mori, S.; Tatsumisago, M. Electrochemical properties of all-solid-state lithium batteries with amorphous MoS_3 electrodes prepared by mechanical milling. *J. Mater. Chem. A* **2015**, *3*, 14142–14147.

(5) Matsuyama, T.; Deguchi, M.; Hayashi, A.; Tatsumisago, M.; Ozaki, T.; Togawa, Y.; Mori, S. Structure Analyses of Amorphous MoS_3 Active Materials in All-solid-state Lithium Batteries. *Electrochemistry* **2015**, *83*, 889–893.

(6) Ye, H.; Ma, L.; Zhou, Y.; Wang, L.; Han, N.; Zhao, F.; Deng, J.; Wu, T.; Li, Y.; Lu, J. Amorphous MoS_3 as the sulfur-equivalent cathode material for room-temperature Li-S and Na-S batteries. *Proc. Natl. Acad. Sci. U S A* **2017**, *114*, 13091–13096.

(7) Ye, H.; Wang, L.; Deng, S.; Zeng, X.; Nie, K.; Duchesne, P. N.; Wang, B.; Liu, S.; Zhou, J.; Zhao, F. *et al.* Amorphous MoS_3 Infiltrated with Carbon Nanotubes as an Advanced Anode Material of Sodium-Ion Batteries with Large Gravimetric, Areal, and Volumetric Capacities. *Adv. Energy Mater.* **2017**, *7*, 1601602.

(8) Chang, U.; Lee, J. T.; Yun, J.-M.; Lee, B.; Lee, S. W.; Joh, H.-I.; Eom, K.; Fuller, T. F. In Situ Self-Formed Nanosheet MoS_3/Reduced Graphene Oxide Material Showing Superior Performance as a Lithium-Ion Battery Cathode. *ACS nano* **2019**, *13*, 1490–1498.

(9) Mei, J.; Wang, C.; Kong, L.; Liu, X.; Hu, Q.; Zhao, H.; Yang, S. Outstanding Performance of Recyclable Amorphous MoS_3 Supported on TiO_2 for Capturing High Concentrations of Gaseous Elemental Mercury: Mechanism, Kinetics, and Application. *Environ. Sci. Technol.* **2019**, *53*, 4480–4489.

(10) Fu, W.; Yang, S.; Yang, H.; Guo, B.; Huang, Z. 2D amorphous MoS_3 nanosheets with porous network structures for scavenging toxic metal ions from synthetic acid mine drainage. *J. Mater. Chem. A* **2019**, *7*, 18799–18806.

(11) Payen, E.; Kasztelan, S.; Houssenbay, S.; Szymanski, R.; Grimblot, J. Genesis and characterization by laser Raman spectroscopy and high-resolution electron microscopy of supported molybdenum disulfide crystallites. *J. Phys. Chem.* **1989**, *93*, 6501–6506.

(12) Toulhoat, H.; Raybaud, P. *Catalysis by transition metal sulphides: From molecular theory to industrial application*; IFP énergies nouvelles publications; Editions Technip: Paris, France, 2013.

(13) Afanasiev, P.; Jobic, H.; Lorentz, C.; Leverd, P.; Mastubayashi, N.; Piccolo, L.; Vrinat, M. Low-Temperature Hydrogen Interaction with Amorphous Molybdenum Sulfides MoS_x. *J. Phys. Chem. C* **2009**, *113*, 4139–4146.

(14) Deng, Y.; Ting, L. R. L.; Neo, P. H. L.; Zhang, Y.-J.; Peterson, A. A.; Yeo, B. S. Operando Raman Spectroscopy of Amorphous Molybdenum Sulfide (MoS_x) during the Electrochemical Hydrogen Evolution Reaction: Identification of Sulfur Atoms as Catalytically Active Sites for H^+ Reduction. *ACS Catal.* **2016**, *6*, 7790–7798.

(15) Ting, L. R. L.; Deng, Y.; Ma, L.; Zhang, Y.-J.; Peterson, A. A.; Yeo, B. S. Catalytic Activities of Sulfur Atoms in Amorphous Molybdenum Sulfide for the Electrochemical Hydrogen Evolution Reaction. *ACS Catal.* **2016**, *6*, 861–867.

(16) Escalera-López, D.; Lou, Z.; Rees, N. V. Benchmarking the Activity, Stability, and Inherent Electrochemistry of Amorphous Molybdenum Sulfide for Hydrogen Production. *Adv. Energy Mater.* **2019**, *9*, 1802614.

(17) Weber, T.; Muijsers, J. C.; van Wolput, J. H. M. C.; Verhagen, C. P. J.; Niemantsverdriet, J. W. Basic Reaction Steps in the Sulfidation of Crystalline MoO_3 to MoS_2, As Studied by X-ray Photoelectron and Infrared Emission Spectroscopy. *J. Phys. Chem.* **1996**, *100*, 14144–14150.

(18) Diemann, E. Radiale Verteilungsfunktionen. V. Strukturuntersuchungen an nichtkristallinem Molybdäntrisulfid, Wolframtrisulfid und Molybdäntriselenid. *Zeitschrift für anorganische und allgemeine Chemie* **1977**, *432*, 127–135.

(19) Liang, K. S.; Cramer, S. P.; Johnston, D. C.; Chang, C. H.; Jacobson, A. J.; deNeufville, J. P.; Chianelli, R. R. Amorphous MoS_3 and WS_3. *J. Non-Cryst. Solids* **1980**, *42*, 345–356.

(20) Chang, C. H.; Chan, S. S. Infrared and Raman studies of amorphous MoS_3 and poorly crystalline MoS_2. *Journal of Catalysis* **1981**, *72*, 139–148.

(21) Huntley, D. R.; Parham, T. G.; Merrill, R. P.; Sienko, M. J. An EXAFS study of the thermal decomposition of molybdenum trisulfide. *Inorg. Chem.* **1983**, *22*, 4144–4146.

(22) Johnston, D. C.; Jacobson, A. J.; Silbernagel, B. G.; Frysinger, S. P.; Rich, S. M.; Gebhard, L. A. Magnetic susceptibility and electron spin resonance as probes of different magnetic species in MoS_3. *Journal of Catalysis* **1984**, *89*, 244–249.

(23) Chien, F. Z.; Moss, S. C.; Liang, K. S.; Chianelli, R. R. Local and intermediate-range structure of amorphous MoS_3: Model calculation study. *Phys. Rev. B* **1984**, *29*, 4606–4615.

(24) Bhattacharya, R. N.; Lee, C. Y.; Pollak, F. H.; Schleich, D. M. Optical study of amorphous MoS_3: Determination of the fundamental energy gap. *J. Non-Cryst. Solids* **1987**, *91*, 235–242.

(25) Sourisseau, C.; Gorochov, O.; Schleich, D.M. Comparative IR and Raman studies of various amorphous MoS_3 and Li_xMoS_3 phases. *Mater. Sci. Eng.* **1989**, *3*, 113–117.

(26) G.F. Khudorozhko, I.P. Asanov, L.N. Maealov, E.A. Kravtsova. The study of electronic structure of molybdenum and tungsten trisulfides and their lithium intercalates by x-ray electron and x-ray emission and absorption spectroscopy. *J. Electron Spectrosc.* **1994**, *68*, 199–209.

(27) Weber, T.; Muijsers, J. C.; Niemantsverdriet, J. W. Structure of Amorphous MoS_3. *J. Phys. Chem.* **1995**, *99*, 9194–9200.

(28) Hibble, S. J.; Rice, D. A.; Pickup, D. M.; Beer, M. P. Mo K-edge EXAFS and S K-edge absorption studies of the amorphous molybdenum sulfides $MoS_{4.7}$, MoS_3, and $MoS_3.nH_2O$ (n ~ 2). *Inorg. Chem.* **1995**, *34*, 5109–5113.

(29) Hibble, S. J.; Walton, R. I.; Pickup, D. M.; Hannon, A. C. Amorphous MoS_3: Clusters or chains? The structural evidence. *J. Non-Cryst. Solids* **1998**, *232-234*, 434–439.

(30) Hibble, S. J.; Feaviour, M. R.; Almond, M. J. Chemical excision from amorphous MoS_3; a quantitative EXAFS study. *J. Chem. Soc., Dalton Trans.* **2001**, 935–940.

(31) Hédoire, C.-E.; Cadot, E.; Villain, F.; Davidson, A.; Louis, C.; Breysse, M. Preparation and characterization of molybdenum sulfide supported on β-zeolites obtained from $[Mo_3S_4(H_2O)_9]^{4+}$ precursor. *Appl. Catal. A* **2006**, *306*, 165–174.

(32) Wang, J.; Ng, S. H.; Chew, S. Y.; Wexler, D.; Wang, G. X.; Liu, H. K. Characterization of Nanosize Molybdenum Trisulfide for Lithium Batteries and MoS_3 Structure Confirmation via Electrochemistry. *Electrochem. Solid State Lett.* **2007**, *10*, A204-A207.

(33) Lassalle-Kaiser, B.; Merki, D.; Vrubel, H.; Gul, S.; Yachandra, V. K.; Hu, X.; Yano, J. Evidence from in situ X-ray absorption spectroscopy for the involvement of terminal disulfide in the reduction of protons by an amorphous molybdenum sulfide electrocatalyst. *J. Am. Chem. Soc.* **2015**, *137*, 314–321.

(34) Müller, A.; Diemann, E.; Krickemeyer, E.; Walberg, H. J.; Bögge, H.; Armatage, A. $[Mo_3(IV)S(S_2)_6]^{2-}$ from amorphous MoS_3 by the reaction with OH^- and R= 0.015 strucutre of $(NH_4)_2[Mo_3(IV)S(S_2)_6]$. *Eur. J. Solid State Inorg. Chem.* **1993**, *30*, 565–572.

(35) Jiao, H.; Li, Y.-W.; Delmon, B.; Halet, J.-F. The Structure and Possible Catalytic Sites of Mo_3S_9 as a Model of Amorphous Molybdenum Trisulfide: A Computational Study. *J. Am. Chem. Soc.* **2001**, *123*, 7334–7339.

(36) Cramer, S. P.; Liang, K. S.; Jacobson, A. J.; Chang, C. H.; Chianelli, R. R. EXAFS studies of amorphous molybdenum and tungsten trisulfides and triselenides. *Inorg. Chem.* **1984**, *23*, 1215–1221.

(37) Hibble, S. J.; Wood, G. B. Modeling the structure of amorphous MoS_3: a neutron diffraction and reverse Monte Carlo study. *J. Am. Chem. Soc.* **2004**, *126*, 959–965.

(38) Khudorozhko, G. F.; Asanov, I. P.; Mazalov, L. N.; Kravtsova, É. A.; Parygina, G. K.; Fedorov, V. E.; Mironov, Y. V. X-ray photoelectron, emission, and absorption studies of the electronic structure of molybdenum and tungsten trisulfides and their intercalates. *J. Struct. Chem.* **1994**, *35*, 823–833.

(39) Li, Y.; Yu, Y.; Huang, Y.; Nielsen, R. A.; Goddard, W. A.; Li, Y.; Cao, L. Engineering the Composition and Crystallinity of Molybdenum Sulfide for High-Performance Electrocatalytic Hydrogen Evolution. *ACS Catal.* **2015**, *5*, 448–455.

(40) Baloglou, A.; Ončák, M.; Grutza, M.-L.; van der Linde, C.; Kurz, P.; Beyer, M. K. Structural Properties of Gas Phase Molybdenum Sulfide Clusters $[Mo_3S_{13}]^{2-}$, $[HMo_3S_{13}]^-$, and $[H_3Mo_3S_{13}]^+$ as Model Systems of a Promising Hydrogen Evolution Catalyst. *J. Phys. Chem. C* **2019**, *123*, 8177–8186.

(41) Kresse, G.; Hafner, J. Ab initio molecular dynamics for liquid metals. *Phys. Rev. B* **1993**, *47*, 558–561.

(42) Kresse, G.; Furthmüller, J. Efficient iterative schemes for ab initio total-energy calculations using a plane-wave basis set. *Phys. Rev. B* **1996**, *54*, 11169–11186.

(43) Kresse, G.; Furthmüller, J. Efficiency of ab-initio total energy calculations for metals and semiconductors using a plane-wave basis set. *Comput. Mater. Sci.* **1996**, *6*, 15–50.

(44) Perdew, J. P.; Burke, K.; Ernzerhof, M. Generalized Gradient Approximation Made Simple. *Phys. Rev. Lett.* **1996**, *77*, 3865–3868.

(45) Steinmann, S. N.; Corminboeuf, C. A generalized-gradient approximation exchange hole model for dispersion coefficients. *J. Chem. Phys.* **2011**, *134*, 44117.

(46) Steinmann, S. N.; Corminboeuf, C. Comprehensive Benchmarking of a Density-Dependent Dispersion Correction. *J. Chem. Theory Comput.* **2011**, *7*, 3567–3577.

(47) Kresse, G.; Joubert, D. From ultrasoft pseudopotentials to the projector augmented-wave method. *Phys. Rev. B* **1999**, *59*, 1758–1775.

(48) Karhánek, D.; Bučko, T.; Hafner, J. A density-functional study of the adsorption of methane-thiol on the (111) surfaces of the Ni-group metals: II. Vibrational spectroscopy. *J. Phys. Condens. Matter.* **2010**, *22*, 265006.

(49) Slater, J. C. Statistical Exchange-Correlation in the Self-Consistent Field. In *Advances in Quantum Chemistry*; Löwdin, P.-O., Ed.; Academic Press, 1972; pp 1–92.

(50) Janak, J. F. Proof that $\partial E/\partial n_i = \varepsilon$ in density-functional theory. *Phys. Rev. B* **1978**, *18*, 7165–7168.

(51) Pueyo Bellafont, N.; Viñes, F.; Hieringer, W.; Illas, F. Predicting core level binding energies shifts: Suitability of the projector augmented wave approach as implemented in VASP. *J. Comput. Chem.* **2017**, *38*, 518–522.

(52) Ansari, R.; Malakpour, S.; Faghihnasiri, M.; Sahmani, S. An ab initio investigation into the elastic, structural and electronic properties of MoS_2 nanotubes. *Superlattice Microst.* **2015**, *82*, 188–200.

(53) Chou, S. S.; Sai, N.; Lu, P.; Coker, E. N.; Liu, S.; Artyushkova, K.; Luk, T. S.; Kaehr, B.; Brinker, C. J. Understanding catalysis in a multiphasic two-dimensional transition metal dichalcogenide. *Nat Commun* **2015**, *6*, 141.

(54) C. Sourrisseau; R.Cavagnat; M. Fouassier, and P. Maraval. Electronic, vibrational and resonance Raman spectra of the layered semiconducting compound NbS_3. *J. Raman Spectro.* **1990**, *21*, 337–349.

(55) Rijnsdorp, J.; Jellinek, F. The crystal structure of niobium trisulfide, NbS_3. *J. Solid State Chem.* **1978**, *25*, 325–328.

(56) Schweiger, H.; Raybaud, P.; Kresse, G.; Toulhoat, H. Shape and Edge Sites Modifications of MoS_2 Catalytic Nanoparticles Induced by Working Conditions: A Theoretical Study. *Journal of Catalysis* **2002**, *207*, 76–87.

(57) Lauritsen, J. V.; Kibsgaard, J.; Helveg, S.; Topsøe, H.; Clausen, B. S.; Lægsgaard, E.; Besenbacher, F. Size-dependent structure of MoS_2 nanocrystals. *Nature Nanotech* **2007**, *2*, 53–58.

(58) Kan, M.; Wang, J. Y.; Li, X. W.; Zhang, S. H.; Li, Y. W.; Kawazoe, Y.; Sun, Q.; Jena, P. Structures and Phase Transition of a MoS_2 Monolayer. *J. Phys. Chem. C* **2014**, *118*, 1515–1522.

(59) Huang, Q.; Li, X.; Sun, M.; Zhang, L.; Song, C.; Zhu, L.; Chen, P.; Xu, Z.; Wang, W.; Bai, X. The Mechanistic Insights into the 2H-1T Phase Transition of MoS_2 upon Alkali Metal Intercalation: From the Study of Dynamic Sodiation Processes of MoS_2 Nanosheets. *Adv. Mater. Interfaces* **2017**, *4*, 1700171.

(60) Zhu, J.; Wang, Z.; Yu, H.; Li, N.; Zhang, J.; Meng, J.; Liao, M.; Zhao, J.; Lu, X.; Du, L. *et al.* Argon Plasma Induced Phase Transition in Monolayer MoS_2. *J. Am. Chem. Soc.* **2017**, *139*, 10216–10219.

(61) Huang, H. H.; Fan, X.; Singh, D. J.; Zheng, W. T. First principles study on 2H-1T′ transition in MoS_2 with copper. *Phys. Chem. Chem. Phys.* **2018**, *20*, 26986–26994.

(62) Oumahi, C.; Barros-Bouchet, M. I. de; Le Mogne, T.; Charrin, C.; Loridant, S.; Geantet, C.; Afanasiev, P.; Thiebaut, B. MoS_2 formation induced by amorphous MoS_3 species under lubricated friction. *RSC Adv.* **2018**, *8*, 25867–25872.

(63) Wang, Z. 2H → 1T′ phase transformation in Janus monolayer MoSSe and MoSTe: An efficient hole injection contact for 2H-MoS_2. *J. Mater. Chem. C* **2018**, *6*, 13000–13005.

(64) Jin, Q.; Liu, N.; Chen, B.; Mei, D. Mechanisms of Semiconducting 2H to Metallic 1T Phase Transition in Two-dimensional MoS_2 Nanosheets. *J. Phys. Chem. C* **2018**, *122*, 28215–28224.

(65) Xia, Z.; Tao, Y.; Pan, Z.; Shen, X. Enhanced photocatalytic performance and stability of 1T MoS_2 transformed from 2H MoS_2 via Li intercalation. *Results Phys.* **2019**, *12*, 2218–2224.

Insert Table of Contents artwork here

